Noncontact Measurements of Resonance of Small Round Liquid Surfaces Using Sound Wave to Determine Surface Tension

*Satoshi Tsukahara**

Graduate School of Science, Osaka University, 1-1, Machikaneyama, Toyonaka, Osaka, 560-0043, Japan.

* Corresponding author E-mail: sxt@chem.sci.osaka-u.ac.jp

ABSTRACT: Various methods have been developed for measuring the surface tension of liquids, and the present study proposes a new method for measuring the surface tension of liquids. A small (9 mm in diameter) round liquid surface was excited by sound waves with a common speaker. Nine liquids possessing various physical properties and functional groups were employed, and three resonance frequencies (f_{rs}) were observed for each liquid in a frequency range of 20 – 180 Hz. The resonances were analyzed with a forced oscillation model. In addition, the amplitudes and phases of the resonance oscillations at various positions of the liquid surface were measured, and the whole deformations of the liquid surface were determined. The deformation was compared with the Bessel functions, and the oscillation modes and boundary conditions were decided. Finally,

proportional relationships between f_{rs} and $\sigma^{0.5}\rho^{-0.5}$ (σ: surface tension, ρ: density) with high correlations were obtained, which were supported by a new theoretical equation using hydrodynamics.

INTRODUCTION

The air/liquid interface (the liquid surface) is a plane of discontinuity in the physical properties of a liquid. The surface tension (σ) of a liquid is one of the fundamental physical properties of the liquid. If a liquid is contaminated with surface-active impurities, its surface tension is highly reduced. Thus, the surface tension is also one of the purity indices of liquids. In our lives, surface tension is related to the foaming of water on washing clothes or dishes and the foaming of beer. These bubbles are caused by surface-active substances.

Surface tension is an essential property for surface chemists. When a surfactant shows an adsorption equilibrium to the surface, the σ value decreases with an increase in the surfactant bulk concentration. The surface excess (the surface concentration) of the surfactant can be obtained from the relationship between σ and the bulk concentration by the Gibbs equation. When a surfactant is not dissolved in a sub-phase solvent, a π–A relationship (π, surface pressure; A, area per molecule) is made. The π–A relationship can be used to know the state of the surfactant monolayer on the surface, such as solid phase, liquid-condensed phase, liquid-expanded phase, or gaseous phase. π is equal to $\sigma_0 - \sigma$, where σ_0 is the surface tension of the pure solvent. In addition, surfactant monolayers can be assembled on a flat plate by the well-known Langmuir–Blodgett (LB) film preparation method (LB method). In the LB method, the surface tension is always monitored to keep the state of the monolayers constant.[1]

Various methods have been developed to measure the surface tension, almost all of which are based on the Young–Laplace equation, such as the drop weight method, the hanging drop method,

and the Wilhelmy method.[1,2] These methods measure the force on a curved surface or its related properties (droplet shape, etc.) and some of them use a probe. For example, in the widely employed Wilhelmy method, a small plate is placed on the surface of a solution and the force on the plate is measured to determine the surface tension. This is a simple method, but the contact angle between the plate and the solution is needed to evaluate the surface tension. In the methods using probes, the affinity between the probe and the solution sometimes has a significant effect on the surface tension value, and thus the development of probe-free methods is desirable.

A few methods based on principles other than the Young–Laplace equation have been reported. Lamb derived an equation among surface tension, density, wavenumber, and frequency of the surface tension wave (ripple, capillary wave) generated on a flat and infinitely wide liquid surface.[3] Based on this Lamb's equation, the quasi-elastic laser scattering (QELS) method was developed as a probe-free method for measurements of surface tension.[4-9] In the QELS method, the wavenumber and frequency of the equally spaced waves on a flat and wide liquid surface were measured simultaneously, and the surface tension was obtained. Recently, Nomoto et al. determined surface tension and surface convection simultaneously by an improved QELS method.[6,7] Since the QELS method measures the frequencies in the kHz range and large wavenumbers (small wavelengths), it is suitable for measurements in the micrometer range.[8]

Lamb and Levich reported an equation for the frequency of single droplet oscillation with surface tension and density.[3,10] Ishiwata et al. measured the resonance oscillation of droplets in air excited by an electric field.[11] Bzdek et al. measured the resonance oscillation associated with the fusion of two droplets levitated in air by optical tweezers.[12,13] In addition, Ishida et al. measured the resonance oscillation of droplets placed on a vibrating substrate.[14,15] In these studies, they used

the droplet equation or a similar equation to evaluate the surface tensions. These methods are also probe-free methods.

On the other hand, we investigated standing, unequally spaced waves on a small round liquid surface excited by a dielectric force. We measured the resonance oscillation of the surface and analyzed it with the Bessel functions to evaluate the surface tension.[16] This method is a probe-free method based on a principle that is not one of the above-mentioned principles. Sakai et al. described oscillations on liquid surfaces with an integral of Bessel functions,[17] but we related a specific resonance to a corresponding Bessel function. A hydrodynamic study was recently reported in which a liquid was placed in a large container (diameter 70 mm, depth 22 mm). The container was vibrated, and the Faraday waves generated on the liquid surface were related to Bessel functions, but the effect of gravity is greater than that of surface tension.[18] The present paper is intended to reinforce the inadequate experimental evidences on oscillation modes and boundary conditions in the previous paper, to improve the sensitivity, and to derive new equations and evaluate the results more quantitatively by adding hydrodynamic considerations. It will also be shown that the contribution of surface tension waves is larger than that of gravity waves. Laser light,[17] an electric field,[16] mechanical vibration,[18] and ultrasonic wave[19] have been used as noncontact external forces to deform the liquid surface, but simpler sound waves are employed in the present study.

EXPERIMENTAL SECTION

Liquids. Nine common liquids with various physical properties and functional groups, listed in Table 1, were employed as samples. Water was purified with a Milli-Q system (Direct-Q UV, Millipore), while the other liquids were of analytical reagent grade. The surface tension (σ), density

(ρ), and viscosity (η) of these liquids are given. The suppliers and purities of these liquids are listed in Table S1 in the Supporting Information.

Table 1. Surface tension (σ), density (ρ), and viscosity (η) of used liquids at 25 °C.[20]

No.	Name	σ / mN m^{-1}	ρ / g cm^{-3}	η / mPa s
1	Ethanol	22.0[a]	0.785	1.083
2	4-Methyl-2-pentanone	23.3[b]	0.796	0.546
3	Dodecane	24.9	0.745	1.378
4	D-Limonene	27.3[c]	0.838	0.923
5	*N*,*N*-Dimethylformamide (DMF)	36.4	0.944	0.802
6	Dimethyl sulfoxide	43.0	1.10	1.991
7	Ethylene glycol (EG)	48.0	1.11	16.1[a]
8	Formamide	58.2	1.13	3.302
9	Water	72.6	0.998	0.890

[a] Reference 21, [b] Value at 23.7 °C, [c] Value at 23.1 °C

Apparatus and Methods. To measure the height change of a liquid surface, we employed a detection system similar to that used in the previous study.[16] This system consisted of an inverted microscope (IX-51, Olympus) with a microscope objective (UPlanFl, 10×, Olympus), two optical fibers, a light source (MegaLight 100, Schott; tungsten halogen lamp, power 100 W), and an avalanche photodiode (C5460-01, Hamamatsu Photonics; APD), as shown in Figure 1. A homemade glass microcell (4.5 mm in radius (r_c), 2 mm in depth (d_c)),[16] was filled with just the right amount of liquid to avoid meniscus formation and rising of the liquid central region. This means that the top face of the microcell is at the same level as the liquid surface. The microcell with a liquid was placed on a motorized xy-axis stage (PMG413-R05AR, Suruga Seiki) on the microscope stage. The xy-axis stage was driven by a motor driver (MS-C2, Chuo Precision Industrial). White light from the light source was irradiated by the objective to an arbitrary position

on the flat round liquid surface through one optical fiber (core diameter 1.0 mm). The reflected light was collected by the same objective and introduced into the APD through the other optical fiber (core diameter 300 μm). This system can convert the height change of the liquid surface into a voltage change.[16]

A mylar speaker (MSI28-12R, SPL Limited; diameter 28 mm, impedance 8 Ω) was used to generate sound waves. This speaker was connected to a function generator (FG-4105, IWATSU) and driven with an alternating current (ac) with a peak-to-peak voltage (U_{pp}) of 0.55 – 3.3 V and a frequency (f_{ex}) of 20 – 180 Hz. The speaker was set to a manipulator (M-152, Narishige) on the same xy-stage on the microscope stage with the speaker facing downward. The centers of the speaker and the microcell were aligned, as shown in Figure 1.

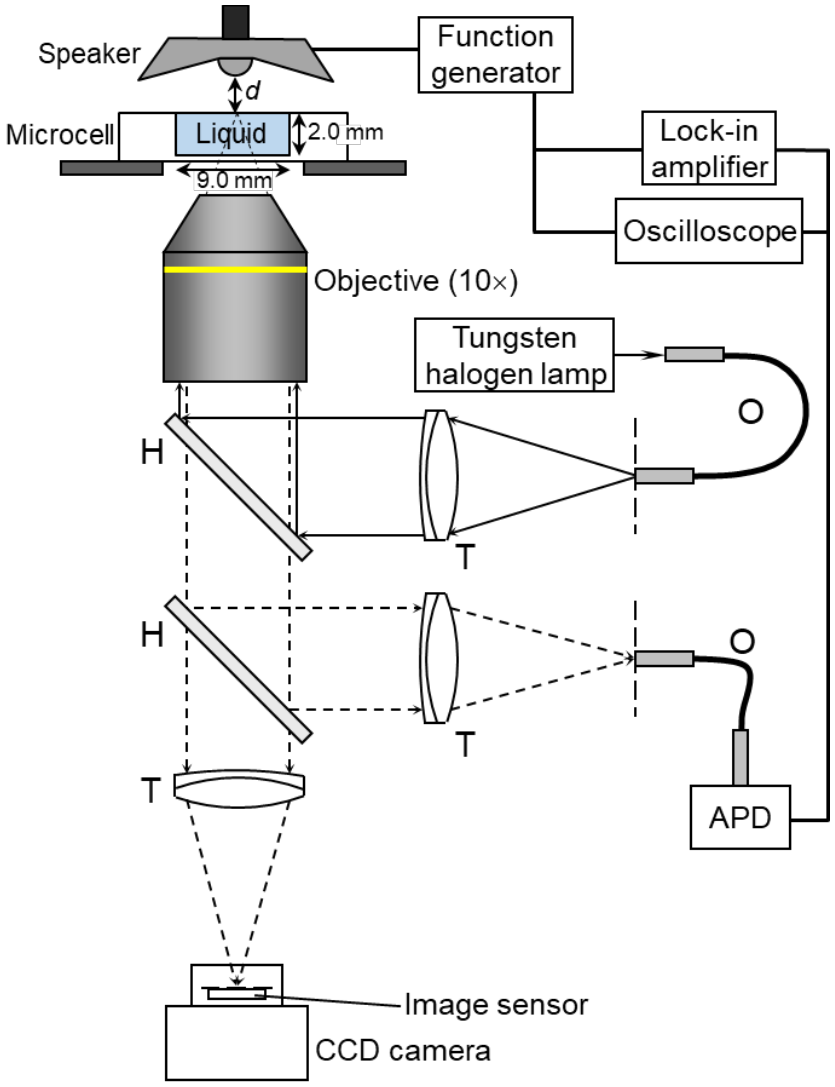

Figure 1. Schematic illustration of the detection system for oscillating the liquid surface with a speaker. *d* is the distance between the bottom of the speaker and the liquid surface. H, Half mirror; O, optical fiber; T, tube lens.

The APD output was connected to a two-phase lock-in amplifier (SR830, SRS) to measure the root-mean-square amplitude (z_{rms}) and phase (φ) of the height change, and it was also connected to an oscilloscope (DS1054Z, RIGOL Technologies) to measure the waveform of the periodic height change (z) of the liquid surface. The output of the function generator was also used as the reference signal for both the lock-in amplifier and the oscilloscope. After applying the ac voltage

to the speaker and waiting at least 1 s, the steady-state height change of the liquid surface was measured. A homemade program written in LabVIEW (National Instruments) controlled the motor driver and the function generator, and the same program also transferred the digital data from the lock-in amplifier and the oscilloscope to a personal computer. All experiments were carried out at 25 ± 1 °C.

RESULTS AND DISCUSSION

Measurements and Analysis of the Liquid Surface Resonances. The height changes of all the liquid surfaces showed sine waves, and their z_{rms} and φ values were measured as a function of f_{ex}. The φ values measured with the lock-in amplifier are in the range of −180° to 180°. Therefore, when the φ increases beyond 180°, it becomes a negative value. In other words, the output φ becomes discontinuous even if the φ changes monotonously. To improve this, 360° was added to the φ in the frequency range higher than the discontinuous point. The details are shown in Section S2 in the Supporting Information. Figures 2a and b illustrate an instance of z_{rms} and φ plots against f_{ex} for the dodecane surface. We successfully measured a few μm-level z_{rms} with the present apparatus. Clearly, there are enhancements in z_{rms} at 33, 68, and 110 Hz. The φ value rises sharply at these frequencies. When U_{pp} applied to the speaker increased, z_{rms} increased but φ did not change.

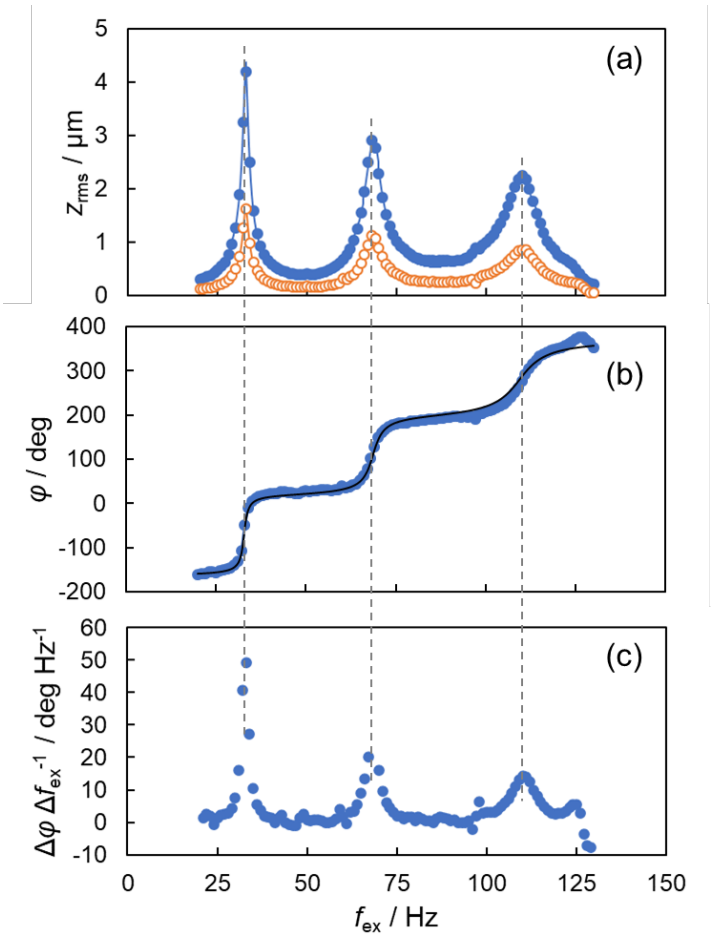

Figure 2. Dependence of (a) z_{rms} (b) φ, and (c) $\Delta\varphi\ \Delta f_{ex}^{-1}$ of the dodecane surface on f_{ex}. d = 1.5 mm, excitation and detection positions: center. U_{pp} = 1.1 V (○), 2.8 V (●). The φ and $\Delta\varphi\ \Delta f_{ex}^{-1}$ values for U_{pp} = 1.1 V were almost the same as those for U_{pp} = 2.8 V, and thus only those for U_{pp} = 2.8 V are shown. The lines in (a) and (b) are regression curves.

At first, the dependencies of z_{rms} and φ were analyzed with equations based on a forced oscillation model.[16,22] The basic equation for a one-dimensional forced oscillation of a substance is:

$$m\frac{d^2z}{dt^2} + c\frac{dz}{dt} + kz = F_{ex}\sin(\omega_{ex}t) \qquad (1)$$

where m is the mass of the substance, z is its displacement, t is time, c is the damping coefficient, k is the spring constant, and F_{ex} is the amplitude of an external force at an angular frequency, ω_{ex} (= $2\pi f_{ex}$). The steady-state solution of eq 1 is:

$$z = z_0 \sin(\omega_{ex} t - \varphi) \tag{2}$$

$$z_0 = \sqrt{2} z_{rms} = \frac{F_{ex}}{\sqrt{(k - m\omega_{ex}{}^2)^2 + c^2 \omega_{ex}{}^2}} \tag{3}$$

$$\varphi = \tan^{-1} \frac{c\,\omega_{ex}}{k - m\omega_{ex}{}^2} \tag{4}$$

Equation 3 corresponds to a single resonance, but we observed three resonances. Therefore, we transformed this equation into the sum of multiple (n) resonances and fit the dependence of z_{rms} in Figure 2a to the resulting eq 5 by the nonlinear least-squares method.

$$z_0 = \sqrt{2} z_{rms} = \sum_n \frac{F_{ex}}{\sqrt{(k_n - m_n \omega_{ex}{}^2)^2 + c_n{}^2 \omega_{ex}{}^2}} + z_{bg} \tag{5}$$

where z_{bg} is the residue. The z_{rms} values calculated with the obtained m_n, c_n, and k_n values (n = 1 – 3) (Section S3 in the Supporting Information) are shown as lines, which reproduce the experimental values well. Equation 4 corresponds to a single resonance, and thus we also transformed this equation into the sum of multiple (n) resonances as eq 6.

$$\varphi = \sum_n \tan^{-1} \frac{c_n\,\omega_{ex}}{k_n - m_n \omega_{ex}{}^2} + \varphi_{bg} \tag{6}$$

where φ_{bg} is the residue. The values calculated with this equation and the parameters obtained from eq 5 are shown as a black line in Figure 2b, which also reproduces the experimental values well.

The resonance angular frequency ($\omega_{rs} = 2\pi f_{rs}$; f_{rs} resonance frequency) of eq 1 is equal to $\sqrt{k/m}$, where the z_{rms} maximum occurs at $\omega_{ex} = \sqrt{k/m - c^2/2m^2}$ from eq 3. In the present study, $k_n/m_n >> c_n{}^2/2m_n{}^2$ for all n (Section S3 in the Supporting Information), and the z_{rms} maximum occurs at almost f_{rs} (= $(1/2\pi)\sqrt{k_n/m_n}$) within 0.3% difference.

In the case of the single resonance, the φ changes from 0° to 180° (maximum change 90°) in the increasing ω_{ex} range around ω_{rs} from eq 4. In the case of the multiple resonances, the second and third φs change from 180° to 360° (maximum change 270°) and from 360° to 540° (maximum change 450°), respectively, from eq 6. Note that φ in the present study was measured based on the voltage applied to the speaker. Since the phase of the sound wave force is 90° advanced from that of the speaker vibration, the theoretical first, second, and third φs of the liquid surface based on the applied voltage change from −90° to 90° (maximum change 0°), 90° to 270° (maximum change 180°), and 270° to 450° (maximum change 360°), respectively. The experimental φ values in Figure 2b were −49°, 103°, and 277° at the resonance frequencies (33, 68, and 110 Hz, respectively), which deviate from the theoretical values. φ includes the transmission process of the sound wave energy to the liquid surface, which may be the cause of the deviation, but the details are unknown. To make the sharp increase in φ more obvious, the φ slope ($\Delta\varphi\ \Delta f_{ex}^{-1}$) was calculated numerically and plotted against f_{ex} in Figure 2c. The frequencies of the z_{rms} maxima exactly agree with those of $\Delta\varphi\ \Delta f_{ex}^{-1}$. Therefore, the resonance phenomenon occurring at the liquid surface is consistent with the one-dimensional forced oscillation theory.

In the case of oscillation of a liquid surface, m, c, and k in eq 1 correspond to ρ, η, and σ of the liquid, respectively.[16] In other words, the f_{rs} depends on σ/ρ and is independent of viscosity. On the other hand, the full width at the $1/\sqrt{2}$-times peak maximum is approximately equal to c_n/m_n,[22] meaning that the higher the viscosity, the broader the peak.

Similar results to Figure 2 were obtained for the other liquids, and the f_{rs} values for the other liquid surfaces were measured in the same way with the centered excitation.

Dependence of z_{rms} on U_{pp} and d. Figure 3a shows a proportional relationship between z_{rms}^2 and U_{pp}^2 at the f_{rs}. It is known that the oscillation energy and the ac electric energy are proportional

to z_{rms}^2 and U_{pp}^2, respectively, indicating that the sound wave energy is converted proportionally to the oscillation energy of the liquid surface. The resonance frequencies are independent of U_{pp} (see Figure 2a), meaning that the intrinsic f_{rs} values were obtained.

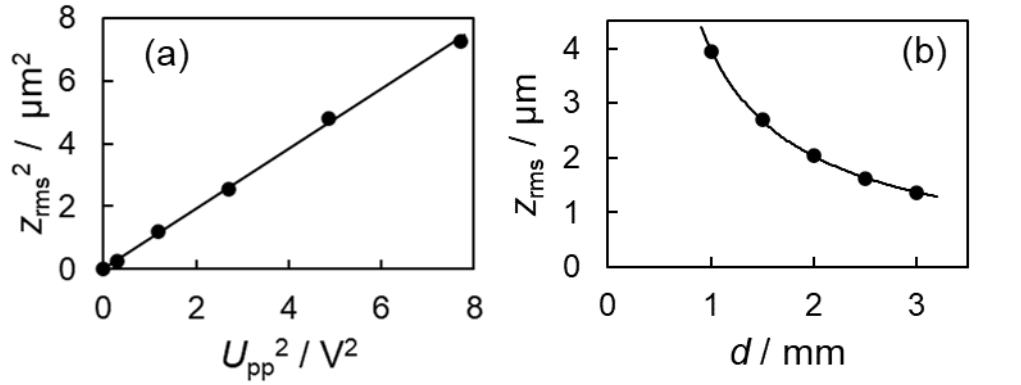

Figure 3. (a) Proportional relationship between z_{rms}^2 of the dodecane surface and U_{pp}^2 applied to the speaker. f_{ex} = 33 Hz, d = 1.5 mm, excitation and detection positions: center. (b) Dependence of z_{rms} of the dodecane surface on d. f_{ex} = 33 Hz, U_{pp} = 2.8 V, excitation and detection positions: center.

We also measured the z_{rms} as a function of the distance (d) between the dodecane surface and the bottom of the speaker (see Figure 1). Figure 3b shows that the z_{rms} decreases with the increase in d, indicating that the sound wave energy diffuses with distance. Similar results to Figure 3 were obtained for the other liquids.

Deformation of Liquid Surface. The speaker and the microcell were moved with the same xy-stage to keep the excitation condition constant, and the z_{rms} and φ of the liquid surface were measured at various positions to know the deformation of the liquid surface. The reproducibility of the position was high, but the accuracy of the position was about ±150 μm.

The f_{rs} values of the DMF surface were already obtained as 35, 74, and 121 Hz. At these frequencies, the z_{rms} and φ were measured at various positions. First, the relationship between z_{rms}

and φ at 35 Hz is shown as a bar graph in Figure 4a. There are only two clusters; the weighted means were −123° ± 6° (cluster α) and 64° ± 6° (cluster β), and their difference is 187° ± 9° (confidence limit with 95% probability). These facts mean that the cluster α is in the same one phase and the cluster β is also in the same other phase, and that the clusters α and β are in opposite phases. In other words, when the surface of the cluster α rises to the top, the surface of the cluster β falls to the valley, and vice versa. In Figure 4b, the normalized z_{rms} and φ are shown as colored circles (red and blue) at the measured positions of the DMF surface. The clusters α and β are shown as red and blue circles, respectively. The color intensity of the circles is proportional to the z_{rms} value. This figure clearly shows a centrosymmetric oscillation. The cluster α (red circle) occupies the center, and the cluster β (blue circle) occupies the outside. The z_{rms} values are almost 0 at the boundary between the clusters α and β, and the location is shown as a green broken line, which corresponds to the oscillation node.

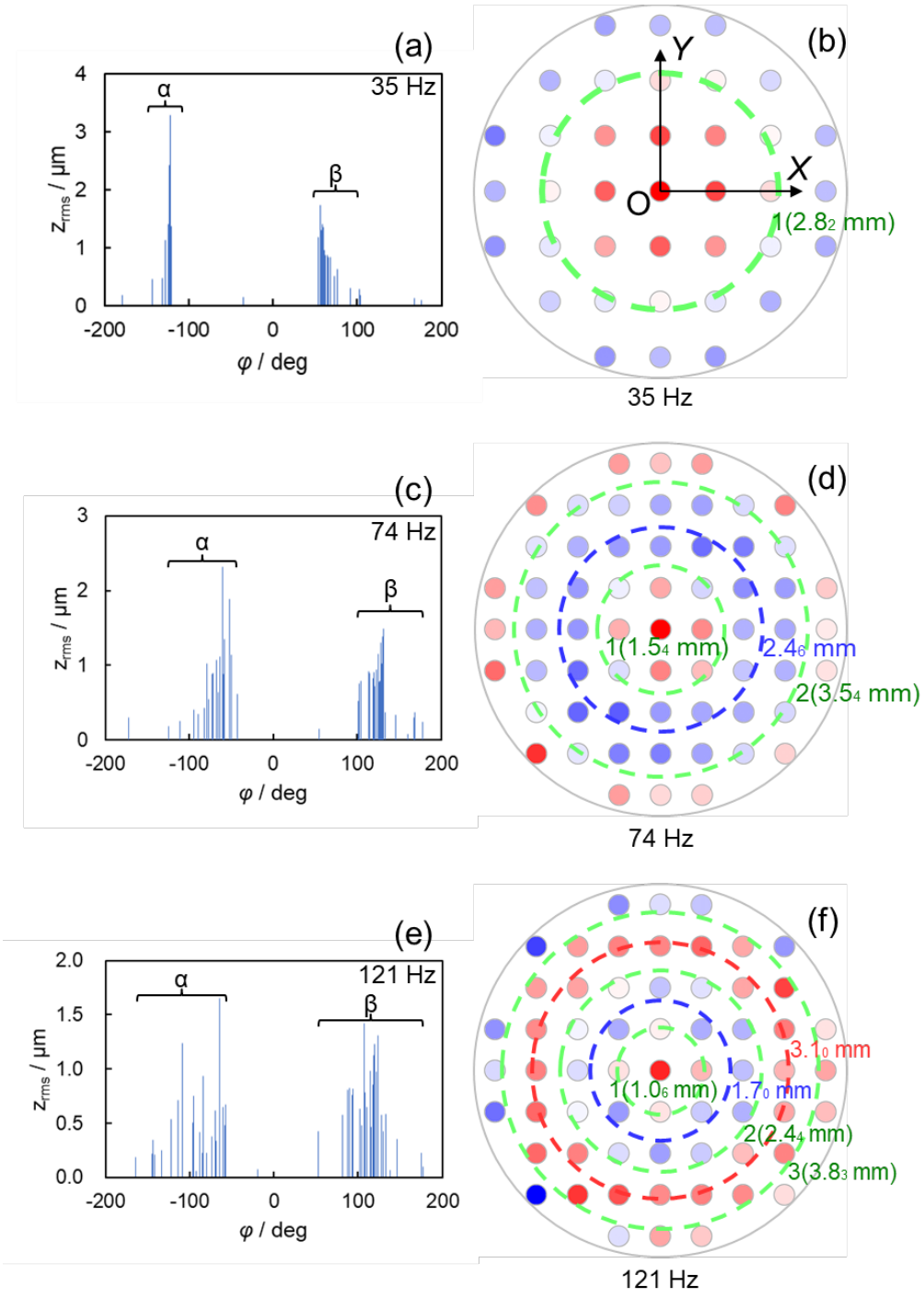

Figure 4. (a,c,e) Relationship between z_{rms} and φ at various positions of the DMF surface at resonance frequencies (35, 74, and 121 Hz, respectively). (b,d,f) Deformation images of the DMF surface at resonance frequencies (35, 74, and 121 Hz, respectively). The green broken lines

represent the nodes, and blue and red broken lines represent the loops. The outermost gray circle represents the DMF edge. U_{pp} = 3.3 V, d = 1.5 mm. The excitation position was centered.

The bar graph between z_{rms} and φ of the DMF surface at 74 and 121 Hz are shown in Figure 4c and 4e, respectively; again, there are only two clusters at these frequencies and their differences are 192° ± 9° and 198° ± 13°, respectively, which are approximately 180°. The deformations at these frequencies are shown in Figure 4d and 4f, respectively. These figures clearly show the centrosymmetric oscillation. Similarly, the nodes are shown as green broken lines. The number of node lines is 2 and 3 for 74 Hz and 121 Hz, respectively.

The speaker and the microcell were moved more finely, and the z_{rms} and φ were measured by changing the detection positions on the X- and Y-axes in Figure 4b. We denoted the distances from the origin (O) as X and Y, respectively. In Figure 5, the z_{rms} is plotted against X or Y where φ belongs to the cluster α, and $(-1)\times z_{rms}$ is plotted where φ belongs to the cluster β. The results on the X- and Y-axes are in good agreement, which means that the oscillation is centrosymmetric again. The zeroth-order Bessel functions of the 1st kind were fit to the results with the least-squares method and the best-fit Bessel functions are shown as green curves. The experimental points are almost identical to the Bessel functions. The best-fit Bessel functions imply that the edge is not a node but an antinode. The Bessel functions that were obtained by fixing the edge to the antinodes of the maximum amplitude with the least-squares method are shown as red lines in Figure 5. The green and red lines are almost identical, indicating that the edge is a loop (an antinode of the maximum amplitude). The positions where z_{rms} = 0 correspond to nodes, which agree well with the green broken lines in Figure 4.

To identify the oscillation mode, information not only at the center but also near the edge is important. As the oscillation mode becomes higher, the distance between the node and the edge

becomes shorter, as shown in Figure 4f and Figure 5c. Therefore, we think that the resolution of the present apparatus does not allow the identification of higher mode deformations.

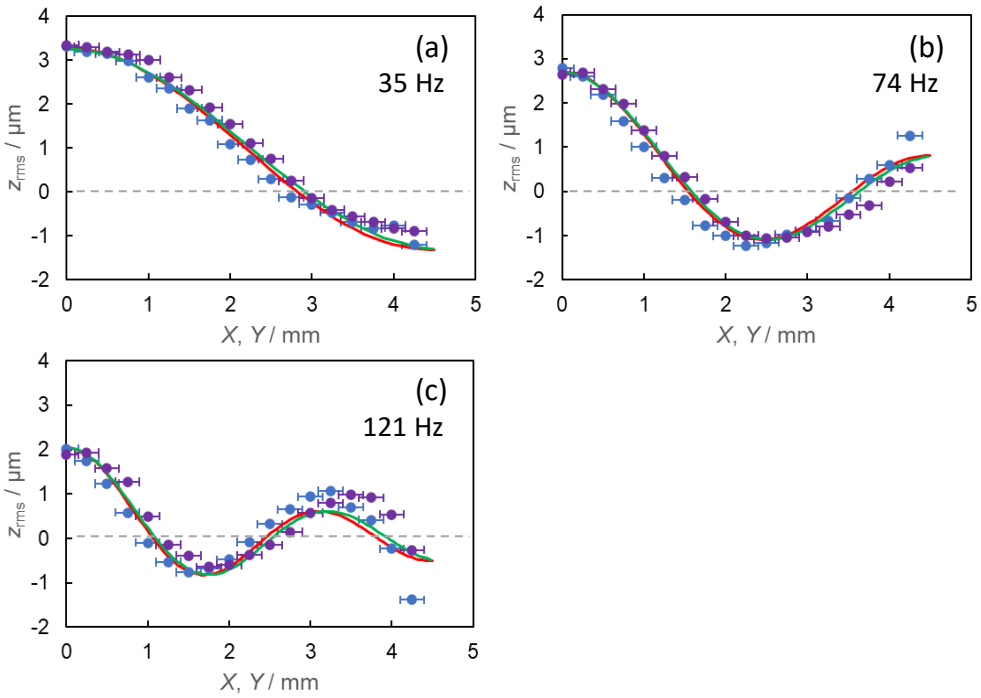

Figure 5. Deformation of the DMF surface at resonance frequencies (a, 35 Hz; b, 74 Hz; c, 121 Hz). (●) *X*, (●) *Y*, (—) best-fit Bessel functions, (—) best-fit Bessel functions obtained by fixing the edge (4.5 mm) to loops. The uncertainties in *X* and *Y* were ±150 µm. U_{pp} = 3.3 V, d = 1.5 mm. The excitation position is centered.

Linear Relationship between f_{rs} and $\sigma^{0.5}\rho^{-0.5}$. We already derived an equation[16] between f_{rs} and $\sigma^{0.5}\rho^{-0.5}$ in the same way as for the two-dimensional round drum, but now we derive a new equation including the hydrodynamic theory as follows. At first, the velocity potential, ϕ, of centrosymmetric and standing waves occurring on a round liquid surface is expressed as:[3,23]

$$\phi(r,z,t) = B\,\frac{\cosh\xi(z+d_c)}{\cosh\xi d_c}\,J_0(\xi r)\cos\omega t \qquad (7)$$

where r is the distance from the center, z is the upward normal axis (z = 0 at the surface), B is a constant, d_c is the depth of the liquid, J_0 is the zeroth-order Bessel function of the 1st kind, and ω is the angular frequency. ξ is equal to $\Lambda(i,j)/r_c$, where $\Lambda(i,j)$ is the eigenvalue related to the oscillation mode (i,j) and r_c is the radius of the round liquid surface. Of course, this ϕ satisfies the equation of continuity for incompressible liquids ($\nabla^2\phi = 0$). From the dynamical boundary condition of the liquid surface,[23]

$$\frac{\partial^2\phi}{\partial t^2} + \left(-\frac{\sigma}{\rho}\frac{\partial^2}{\partial r^2} + g \right)\frac{\partial\phi}{\partial z} = 0 \text{ on } z = 0 \text{ (surface)} \quad (8)$$

where g is the acceleration of gravity. By substituting ϕ of eq 7 into eq 8, f_{rs} is approximately obtained as:

$$f_{rs} \approx \frac{1}{2\pi}\sqrt{\left(\frac{\sigma\xi^3}{\rho} + g\xi \right)\tanh\xi d_c} \quad (9)$$

The detailed derivation is given in Section S4 in the Supporting Information. The present experimental conditions correspond to the deep liquid waves, that is, $\tanh \xi d_c \approx 1$ with ξ (= 0.85, 1.56, and 2.26 mm^{-1}, see the next sentences) and d_c (2 mm) values. Therefore,

$$f_{rs} \approx \frac{1}{2\pi}\sqrt{\frac{\sigma\xi^3}{\rho} + g\xi} \quad (10)$$

In the Lamb's equation and the QELS method, the wavenumber is used instead of ξ in eq 10. As for the surface waves, the surface tension wave (ripples) and the gravity wave are known. Each restoring force is caused by the surface tension and the gravity, respectively. From eq 10, the former is dominant for $\xi > \sqrt{\rho g/\sigma}$ and the latter is dominant for $\xi < \sqrt{\rho g/\sigma}$. The $\sqrt{\rho g/\sigma}$ values were calculated to be 0.36 – 0.59 mm^{-1} for the liquids used, which are smaller than the ξ values. Therefore, we can say that the oscillation of the liquid surfaces in the present study is the surface tension wave. In the followings, we will neglect the contribution of the gravity wave and f_{rs} can be expressed as:

$$f_{rs} \approx \frac{1}{2\pi}\sqrt{\frac{\sigma\Lambda(i,j)^3}{\rho r_c^3}} = C\sqrt{\frac{\sigma}{\rho}}, \quad C = \frac{1}{2\pi}\sqrt{\frac{\Lambda(i,j)^3}{r_c^3}} \tag{11}$$

According to eq 11, we plotted the obtained f_{rs} against $\sigma^{0.5}\rho^{-0.5}$ in Figure 6. We call the 3 groups the 1st, 2nd, and 3rd groups from the lower resonances. This figure shows a proportional relationship with a high correlation for each group, meaning that the oscillations of all liquid surfaces in each group belong to the same oscillation mode. The present 1st group results agree well with the previous ones (gray points).[16] This fact means that the resonances by the dielectric force[16] are the same as those by the sound wave, and that the intrinsic resonances of the liquid surfaces are obtained regardless of the excitation methods. As for EG (No.7), the 3rd f_{rs} cannot be observed. This would be due to its higher viscosity by one order of magnitude (Table 1), which leads to the broadening of the peak width as mentioned above. Figure 2(a) shows that the peak width of the 3rd resonance is wider than those of the 1st and 2nd resonances. These factors would prevent the observation of the 3rd f_{rs} of EG.

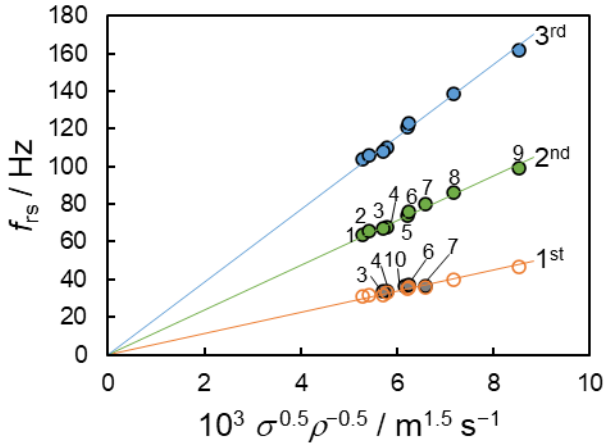

Figure 6. Proportional relationships between f_{rs} and $\sigma^{0.5}\rho^{-0.5}$ for the three groups (○, 1st; ●, 2nd; ●, 3rd). The numbers in the figure correspond to the liquid Nos. in Table 1. The gray plots are the previous results (No.10 *N*-methylformamide).[16]

The i of the oscillation mode is the number of node lines passing through the center, and thus $i = 0$. When the edge is fixed physically, the j is the number of concentric node lines including the edge node.[22] In the present liquid surfaces, however, the edge is not the node but the loop, and therefore j is not an integer. We define j as $1\frac{1}{2}$, $2\frac{1}{2}$, and $3\frac{1}{2}$ for the 1st, 2nd, and 3rd groups, respectively. The $\Lambda(0,1\frac{1}{2})$, $\Lambda(0,2\frac{1}{2})$, and $\Lambda(0,3\frac{1}{2})$ values are obtained as 3.83, 7.02, and 10.17, respectively, from the point where the zeroth-order Bessel functions of the 1st kind shows the maximum amplitude.[24] The C values in eq 11 were calculated with these Λ and r_c (= 4.5 mm) values, and they were plotted against the obtained slope values in Figure 6. The result is shown in Figure 7(a), which means that both are in good agreement.

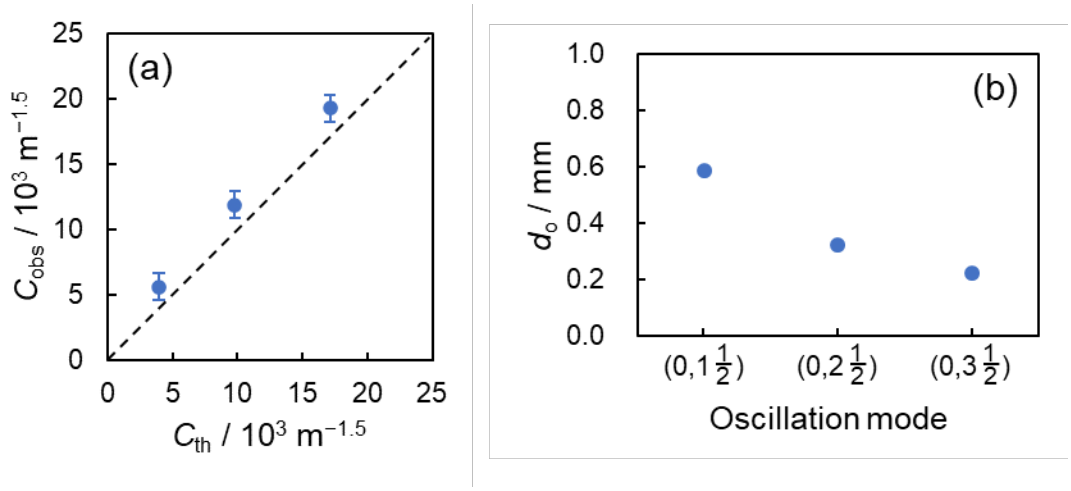

Figure 7. (a) Correlation between the observed slopes (C_{obs}) in Figure 6 and the theoretical slopes (C_{th}) calculated with eq 11. (b) Calculated oscillation depth (d_o) as a function of the oscillation mode.

Motion of Liquid near the Surface. As mentioned above, $\tanh \xi d_c \approx 1$ and thus the velocity potential is simply given from eq 7 as:

$$\phi(r,z,t) \approx B\, e^{\xi z} J_0(\xi r) \cos \omega t \qquad (12)$$

The oscillation amplitudes near a liquid surface in the r and z directions (A_r and A_z) can be expressed from the kinematical boundary condition as:[17,23]

$$A_r \approx \int \frac{\partial \phi}{\partial r} dt = -\frac{B\xi}{\omega} e^{\xi z} J_1(\xi r) \sin \omega t \quad (13)$$

$$A_z \approx \int \frac{\partial \phi}{\partial z} dt = \frac{B\xi}{\omega} e^{\xi z} J_0(\xi r) \sin \omega t \quad (14)$$

where J_1 is the first-order Bessel function of 1st kind. A_r and A_z at the same time ($t = -\pi/2\omega$) are calculated with eqs 13 and 14, and are shown schematically in Figure 8. A_z is analogous to the surface shape. A_r and A_z decay exponentially toward the bottom, and both work to flatten the liquid surface. Only A_r and A_z exist at the nodes and loops, respectively, from the surface to the bottom.

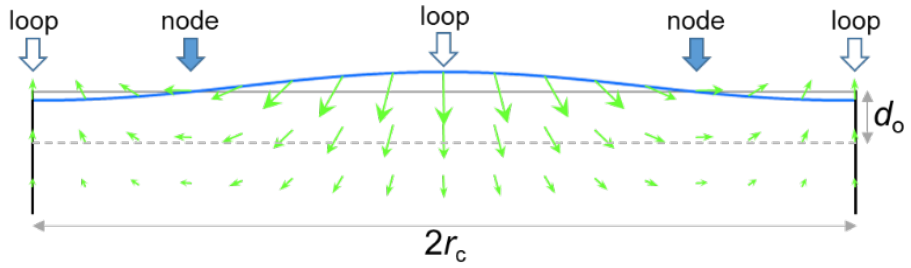

Figure 8. Cross-sectional view of the surface deformation (—) and the motion (oscillation amplitude) of the liquid (→) of the oscillation mode $(0, 1\frac{1}{2})$. The motion decays exponentially from the surface to the bottom. The d_o for the oscillation energy of this oscillation mode is shown as a broken line.

A round drum has a membrane, the edge of which is physically fixed, and thus the edge becomes a node.[22] On the other hand, the edge of the liquid surface cannot be physically fixed. In the present liquid case, the boundary condition is $d\phi/dr = 0$ at $r = r_c$ from the surface to the bottom,[3] and therefore the liquid at the edge moves only vertically along the edge wall in Figure 8, that is, $A_r = 0$. As the result, the edge becomes a loop. This is confirmed with the experimental data (Figures 4 and 5).

Since the oscillation energy is proportional to A_r^2 or A_z^2, its dependence on z is expressed as $e^{2\xi z}$ from eqs 13 and 14. Similar to the penetration depth of the evanescent light wave,[25] the oscillation depth (d_o) is defined as the depth where the oscillation energy decays to 1/e times (e: Napier's constant). d_o is equal to $1/(2\xi)$, and the calculated d_o is shown in Figure 7(b). d_o decreases with the increase in j, because the larger the number of nodes, the smaller the distance between the nodes, as shown in Figure 4, and the shallower the oscillation depth. The microcell used has a depth of 2 mm, which is sufficient compared with the d_o, as shown in Figure 7b. At the bottom of the microcell, the oscillation energy decays by 3%, 0.2%, and 0.01% for the $(0, 1\frac{1}{2})$, $(0, 2\frac{1}{2})$, and $(0, 3\frac{1}{2})$ modes, respectively.

CONCLUSIONS

The center of a small and round liquid surface was excited by a sound wave emitted from a common speaker, and its resonance frequencies (f_{rs}) were measured in the range of 20 – 180 Hz with a microscope-based system. Nine liquids with various physical properties and functional groups were employed as samples, and proportional relationships between f_{rs} and $\sigma^{0.5}\rho^{-0.5}$ were obtained with a high correlation. In addition, the oscillation amplitude and phase at f_{rs} were measured at different positions on the liquid surface, and the deformation of the liquid surface was obtained. From the deformation information, the centrosymmetric oscillation modes of the liquid surface, $(0, 1\frac{1}{2})$, $(0, 2\frac{1}{2})$, and $(0, 3\frac{1}{2})$, were identified. Finally, an equation based on the hydrodynamics has been successfully given to the above proportional relationships for the first time.

It is difficult to measure the deformation of higher-order oscillation modes with the resolution of the present system, and therefore it will be necessary to develop a new measurement system with new concepts and means, such as imaging, that has higher resolution.

The proportional relationship between f_{rs} and $\sigma^{0.5}\rho^{-0.5}$ obtained in this study, which is independent of the other physical properties and functional groups of liquids, means that this relationship would become a new method for measuring surface tension because the density of liquids is easy to measure. This method requires only 130 μL of liquid, and the microcell used is the appropriate size to be manually filled with a liquid; it is a feature not found in other methods. Therefore, it is expected to be applied in the future to extremely valuable samples, such as biological samples or solutions of substances that are difficult to synthesize.

ASSOCIATED CONTENT

Supporting Information.

The supporting Information is available free of charge.

AUTHOR INFORMATION

Corresponding Author

*Satoshi Tsukahara. Graduate School of Science, Osaka University, 1-1, Machikaneyama, Toyonaka, Osaka, 560-0043, Japan; orcid.org/0000-0002-6998-4103; Phone: +81-6-6850-5411; Email: sxt@chem.sci.osaka-u.ac.jp

Funding Sources

This study was supported by the JSPS KAKENHI grant No. 17H03078.

Notes

The author declares no competing financial interest.

ABBREVIATIONS

LB, Langmuir–Blodgett; QELS, quasi-elastic laser scattering; DMF, *N*,*N*-dimethylformamide; EG, ethylene glycol; APD, avalanche photodiode.

REFERENCES

(1) Kondo, T. *Shinpan Kaimen Kagaku (Newly-Published Surface Chemistry, in Japanese)*; Sankyo Shuppan Co., Ltd., Tokyo, 2001.

(2) Tsukahara, S. Recent Analytical Methodologies on Equilibrium, Kinetics, and Dynamics at Liquid/Liquid Interface. *Anal. Chim. Acta* **2006**, *556* (1), 16–25. DOI: 10.1016/j.aca.2005.05.050.

(3) Lamb, H. *Hydrodynamics*, 6th ed.; Dover Publications, New York, 1945.

(4) Sakai, K.; Tanaka, H.; Takagi, K. Dispersion of Thermal Ripplon on Free Surfaces of Pure Liquids Measured up to 6 Mhz. *Jpn. J. Appl. Phys.* **1990**, *29* (12), L2247–L2249. DOI: 10.1143/JJAP.29.L2247.

(5) Tsuyumoto, I.; Uchikawa, H. A High-Performance and Simplified Quasi-Elastic Laser Scattering Method Using Homodyne Detection in Beam Divergence. *Anal. Chem.* **2001**, *73* (10), 2366–2368. DOI: 10.1021/ac001338e.

(6) Nomoto, T.; Marumo, M.; Chiari, L.; Toyota, T.; Fujinami, M. Time-Resolved Measurements of Interfacial Tension and Flow Speed of the Inclined Water Surface around a Self-Propelled Camphor Boat by the Quasi-Elastic Laser Scattering Method. *J. Phys. Chem. B* **2023**, *127* (12), 2863–2871. DOI: 10.1021/acs.jpcb.3c00466.

(7) Nomoto, T.; Kimura, H.; Chiari, L.; Toyota, T.; Fujinami, M. Flow-Driven Self-Propulsion of Oil Droplet on a Surfactant Solution Surface, as Observed by Time-Resolved Interfacial

Tension and Surface Flow Speed Measurements. *Langmuir* **2024**, *40* (8), 4468–4474. DOI: 10.1021/acs.langmuir.3c03857.

(8) Hibara, A. Optical Surface Tension Measurement Method for Microscale Liquid. *Bunseki Kagaku* **2023**, *72* (3), 79–86. DOI: 10.2116/bunsekikagaku.72.79

(9) Chung, M.; Pigot, C.; Volz, S.; Hibara, A. Optical Surface Tension Measurement of Two-Dimensionally Confined Liquid Surfaces. *Anal. Chem.* **2017**, *89* (15), 8092–8096. DOI: 10.1021/acs.analchem.7b01611.

(10) Levich, V. G. *Physicochemical Hydrodynamics*; Prentice-Hall, Inc., Englewood Cliffs, N.J., 1962.

(11) Ishiwata, T.; Sakai, K. Dynamic Surface Tension Measurement with Temporal Resolution on Microsecond Scale. *Appl. Phys. Express* **2014**, *7* (7), 077301. DOI: 10.7567/APEX.7.077301.

(12) Bzdek, B. R.; Collard, L.; Sprittles, J. E.; Hudson, A. J.; Reid, J. P. Dynamic Measurements and Simulations of Airborne Picolitre-Droplet Coalescence in Holographic Optical Tweezers. *J. Chem. Phys.* **2016**, *145* (5), 054502. DOI: 10.1063/1.4959901.

(13) Boyer, H. C.; Bzdek, B. R.; Reid, J. P.; Dutcher, C. S. Statistical Thermodynamic Model for Surface Tension of Organic and Inorganic Aqueous Mixtures. *J. Phys. Chem. A* **2017**, *121* (1), 198–205. DOI: 10.1021/acs.jpca.6b10057.

(14) Ishida, S.; Mitani, S.; Sakai, K. High Speed Measurement of Liquid Properties from Behavior of Micro Droplets on Vertically Oscillating Substrate. *Jpn. J. Appl. Phys.* **2023**, *62*, SJ8001. DOI: 10.35848/1347-4065/acaf75.

(15) Ishida, S.; Mitani, S.; Sakai, K. Experimental and Theoretical Research on Oscillation Behavior of Droplets on Horizontally Oscillating Substrates. *Jpn. J. Appl. Phys.* **2024**, *63* (3), 03SP02. DOI: 10.35848/1347-4065/ad1e9c.

(16) Tsukahara, S.; Tsuruta, T.; Fujiwara, T. Surface Tension Determination through Measurements of Resonance Oscillation of a Small Surface Using Dielectric Force by a Localized Alternating Current Electric Field. *Analyst* **2013**, *138* (7), 2110–2117. DOI: 10.1039/c3an36260d.

(17) Sakai, K.; Mizuno, D.; Takagi, K. Measurement of Liquid Surface Properties by Laser-Induced Surface Deformation Spectroscopy. *Phys. Rev. E* **2001**, *63* (4), 046302. DOI: 10.1103/PhysRevE.63.046302.

(18) Shao, X.; Wilson, P.; Saylor, J. R.; Bostwick, J. B. Surface Wave Pattern Formation in a Cylindrical Container. *J. Fluid Mech.* **2021**, *915*, A19. DOI: 10.1017/jfm.2021.97.

(19) Sisombat, F.; Devaux, T.; Haumesser, L.; Callé, S. Contactless Deformation of Fluid Interfaces by Acoustic Radiation Pressure. *Sci. Rep.* **2023**, *13* (1), 14703. DOI: 10.1038/s41598-023-39464-0.

(20) Riddick, J. A.; Bunger, W. B.; Sakano, T. K. *Organic Solvents: Physical Properties and Methods of Purification*, 4th ed.; John Wiley & Sons, Inc., New York, 1986.

(21) *CRC Handbook of Chemistry and Physics*, 89th ed.; Lide, D. R., Ed.; CRC Press, Inc. Boca Raton, 2008.

(22) Tokuoka, T. *Shindo-Ron (Oscillation Theory in Japanese)*; Saiensu-sha Co., Ltd., Tokyo, 1984.

(23) Suzuki, K. *Hydrodynamics and Theory of Fluid Resistance (in Japanese)*; Seizando-Shoten Publishing Col. Ltd., Tokyo, 2010.

(24) *Casio Calculation site.* https://keisan.casio.jp/exec/system/1161228678 (accessed 2024-07-15).

(25) Hansen, W. N. *"Internal Reflection Spectroscopy in Electrochemistry" in Advances in Electrochemistry and Electrochemical Engineering, Vol. 9*; Tobias, C. W., Ed.; John Wiley & Sons Inc., New York, 1973.

For Table of Contents Only

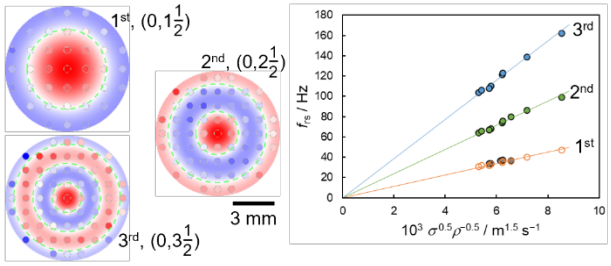

Oscillation modes of liquid surface and proportional relation between the resonance frequency (f_{rs}) and $\sigma^{0.5}\rho^{-0.5}$ (σ: surface tension, ρ: density)